



1 **Landslide displacement prediction using the GA-LSSVM model and time series analysis: a case study**
2 **of Three Gorges Reservoir, China**

3 Tao Wen¹, Huiming Tang^{1,2*}, Yankun Wang², Chengyuan Lin¹, Chengren Xiong²

4 ¹ Faculty of Engineering, China University of Geosciences, Wuhan 430074, Hubei, People's Republic of China; ² Three Gorges
5 Research Center for Geo-hazards of Ministry of Education, China University of Geosciences, Wuhan, Hubei 430074, People's
6 Republic of China

7 *Corresponding author: tanghm@cug.edu.cn
8

9 **Abstract** Predicting landslide displacement is challenging, but accurate predictions can prevent casualties and economic losses.
10 Many factors can affect the deformation of a landslide, including the geological conditions, rainfall, and reservoir water level.
11 Time series analysis was used to decompose the cumulative displacement of landslide into a trend component and a periodic
12 component. Then the least squares support vector machine (LSSVM) model and genetic algorithm (GA) were used to predict
13 landslide displacement, and we selected a representative landslide with step-like deformation as a case study. The trend
14 component displacement, which is associated with the geological conditions, was predicted using a polynomial function, and the
15 periodic component displacement which is associated with external environmental factors, was predicted using the GA-LSSVM
16 model. Furthermore, based on a comparison of the results of the GA-LSSVM model and those of other models, the GA-LSSVM
17 model was superior to other models in predicting landslide displacement, with the smallest root mean square error (*RMSE*), mean
18 absolute error (*MAE*), and mean absolute percentage error (*MAPE*). The results of the case study suggest that the model can
19 provide good consistency between measured displacement and predicted displacement, and periodic displacement exhibited good
20 agreement with trends in the major influencing factors.

21 **Keywords** landslide; displacement prediction; least squares support vector machine; genetic algorithm; reservoir water level;
22 rainfall
23

24 **1 Introduction**

25 In the Three Gorges Reservoir region, landslides are the main type of geo-hazard, and they cause critical harm to individuals
26 and property each year (Du et al. 2013; Yao et al. 2013; Lian et al. 2014; Cao et al. 2016). Therefore, geological surveying,
27 monitoring, landslide prevention and landslide prediction must be improved to mitigate the losses caused by landslides
28 (Kirschbaum et al. 2010; Miyagi et al. 2011; Ahmed 2013). A landslide can be regarded as a nonlinear and dynamic system that is
29 affected by external factors, such as geological conditions, rainfall, reservoir water levels, groundwater, etc. (Guzzetti et al. 2005;
30 Kawabata and Bandibas 2009). Due to the influences of external factors, deformation displacement of landslide generally exhibits
31 the same tendencies as the variations in external factors, which can result in misleading landslide prediction. The displacement
32 prediction of landslides is a major focus in the field of landslide research (Sassa et al. 2009; Du et al. 2013). Comprehensive
33 analyses of landslide response and displacement predictions of landslide based on external factors are effective methods that rely
34 on landslide deformation data. The accurate prediction of reservoir landslide processes is an important basis for early prevention,
35 and it can reduce the loss of property and lives (Corominas et al. 2005).

36 In recently years, grey system models, time series models, neural network models, extreme learning machines, support
37 vector machines (SVM), etc. have been widely used for landslide displacement prediction (Wang 2003; Pradhan et al. 2014;
38 Gelisli et al. 2015; Goetz et al. 2015; Kavzoglu et al. 2015). Previously, landslide susceptibility maps were assessed using a back
39 propagation artificial neural network and logistic regression analysis (Nefeslioglu et al. 2008). Additionally, dynamic time series
40 predictors were proposed based on echo state networks (Yao et al. 2013). Lian et al. (2013) used an extreme learning machine and
41 ensemble empirical mode decomposition to predict landslide displacement. Although these models were constructed based on
42 different algorithms, each has strengths and weaknesses. Grey system models are widely used in analyses of exponential time
43 series. However, for complex nonlinear slope displacement series, prediction results can yield considerable error (Yin and Yu 2007;
44 Sun et al. 2008). Additionally, autocorrelation coefficients, partial correlation coefficients and pattern recognition features are
45 difficult to determine via time series analysis (Brockwell and Davis 2013; Turner et al. 2015). The neural network method is a



1 powerful tool in landslide prediction (Liu et al. 2014; Lian et al. 2015). However, the conventional neural network has many
2 limitations, including overfitting and a shortage of theoretical guidance in the selection of the number of network nodes in the
3 hidden layer, which diminishes its prediction ability (Hwang et al. 2014). In addition, the neural network neglects practical issues
4 by using a pre-defined activation function. Compared with traditional learning algorithms, although extreme learning machines
5 are characterized by high generalization, good performance and fast computing speed, their output is different at different times
6 due to the use of randomly selected input (Lian et al. 2014). Thus, it is difficult to reflect large quantities of information
7 completely and predict landslide displacement accurately using these models because landslide displacement is actually a finite
8 time series.

9 The SVM model has strong generalization ability and can effectively overcome the limitations of other methods, including
10 small sample sizes, high dimensionality and nonlinearity. Many studies have illustrated the ability of SVM models to recognize
11 learning patterns, such as nonlinear regression, and obtain the global optimum solutions to these problems (Feng et al. 2004;
12 Marjanović et al. 2011; Micheletti et al. 2011; Hong et al. 2016). Although these problems can be transformed into quadratic
13 convex programming problems, the computation speed of the SVM model is slow when the training data set is large or the
14 dimensionality is high (Zhang et al. 2009). To overcome these inadequacies, we use the least squares support vector machine
15 (LSSVM) proposed by Suykens and Vandewalle (1999), which is a supervised learning model that has been widely applied in
16 other machine learning problems, such as function fitting. The LSSVM model uses the square sum of the least square linear
17 system error as the loss function and solves the problem by transforming it into a set of equations, which increases the solution
18 speed and reduces the required calculation resources (Suykens et al. 2002; Lv et al. 2013; Xu and Chen 2013; Zhang et al. 2013).
19 Additionally, this method yields good performance in pattern recognition and nonlinear function fitting. However, the selection of
20 parameters is crucial to developing an efficient LSSVM model due to its sensitivity to small variations in the parameters.

21 The genetic algorithm (GA) is a global optimization algorithm that uses highly parallel, random and adaptive searching
22 based on biological natural selection and optimization. Thus, the method is particularly suitable for solving complex and nonlinear
23 problems (Li et al. 2010; Ali et al. 2013). In this paper, the GA is selected as the method of parameter optimization in the LSSVM
24 due to its advantages in determining the unknown parameters that have great consistent between the predicted data and the
25 measured data. By introducing the GA, some key parameters of the LSSVM model can be ascertained automatically. Therefore,
26 we select the combination of the LSSVM model and the GA to predict landslide displacement.

27 Due to the influences of rainfall, reservoir water level and human activities on the monitoring data of landslide displacement,
28 most monitoring data series are incomplete or highly variable. These issues introduce uncertainty into the mathematical model and
29 increase the difficulty of prediction. To overcome this shortcoming and obtain the main error sources, a time series analysis of
30 displacement is conducted by decomposing the monitoring data series into several components (Du et al. 2013). Then, the
31 monitoring data series are simulated using the moving average method. This paper is organized as follows. The GA-LSSVM
32 model with time series analysis is described in Section 2. Taking a typical landslide with step-like deformation as an example,
33 details of the case study are introduced in Section 3. Model validation results based on landslide displacement prediction and the
34 prediction results of the GA-LSSVM model and other models are given in Section 4.

35 **2 Methodology**

36 **2.1 Time series analysis of displacement**

37 Cumulative displacement of landslide is caused by the joint effects of geological conditions (lithology, geological structure,
38 topography, etc.) and external environmental factors (rainfall, reservoir water level, etc.). The landslide displacement caused by
39 the former increases monotonically with time, which reflects the trend in cumulative displacement. However, the landslide
40 displacement induced by the latter is approximately periodic. Therefore, a landslide displacement sequence is an instability time
41 series with a periodic step-like characteristic. According to time series analysis, cumulative displacement can be decomposed into
42 three portions as follows:

$$43 \quad y_t = p_t + q_t + \varepsilon_t \quad (1)$$

44 where y_t is the cumulative displacement, p_t is the trend component displacement, q_t is the periodic component displacement,



1 and ε_t is the random component displacement.

2 However, it is difficult to obtain relevant data regarding the random component (wind loads, car loads, etc.) due to the lack
 3 of advanced monitoring methods. In this paper, the random component displacement is not considered. Therefore, we can simplify
 4 the time series model as follows.

$$5 \quad y_t = p_t + q_t \quad (2)$$

6 The trend component can be extracted using the moving average method as follows:

$$7 \quad A_i = \{a_1, a_2, \dots, a_j, \dots, a_n\} \quad (3)$$

$$8 \quad \bar{p}_t = \frac{a_t + a_{t-1} + \dots + a_{t-k+1}}{k} \quad (t = k, k+1, \dots, n) \quad (4)$$

9 where A_i is the time series of cumulative displacement of the i th monitoring system ($i=1, 2, \dots, m$), a_j is the cumulative
 10 displacement of the i th monitoring system at time j ($j=1, 2, \dots, n$), \bar{p}_t is the extracted value of the trend component, and k is the
 11 moving average period.

12 The periodic component displacement can be acquired by subtracting the trend component displacement from the
 13 cumulative displacement. Therefore, the time series model not only reflects the relationship between each component of
 14 cumulative displacement but also provides mathematical and physical meaning for landslide displacement prediction.

15 2.2 LSSVM

16 The LSSVM model is a regression prediction method with nonlinear characteristics based on a statistical learning theory,
 17 and it is regarded as an improved form of the SVM (Vapnik 1995; Abdi and Giveki 2013). First, after dividing the sample data
 18 into training samples and testing samples, the training samples are plotted in a high-dimension feature space via nonlinear
 19 mapping. Then, the optimal decision function model is obtained for the best-fitted results by training the sample data $\{x_j, y_j\}$,
 20 where $j=1, 2, 3, \dots, n$. The regression function of the LSSVM can be expressed as follows:

$$21 \quad f(x) = W^T \varphi(x) + b \quad (5)$$

22 where W^T is the weight vector, $\varphi(x)$ is a nonlinear mapping function that maps the sample data into the feature space, x is the
 23 input, y is the output, and b is the offset.

24 By searching for a function $f(x)$ that adjusts the dispersion degree of the training samples, we can obtain a risk-minimized
 25 solution. This solution can be written using the structural risk minimization principle:

$$26 \quad \text{Minimize: } \frac{1}{2} W^T W + \frac{C}{2} \sum_{j=1}^n \xi_j^2 \quad (6)$$

$$27 \quad \text{Subject to: } y_j = W^T \varphi(x_j) + b + \xi_j \quad (j = 1, 2, \dots, n) \quad (7)$$

28 where C is a penalty factor representing the penalty degree of the training samples, b is the offset, and ξ_j is the relaxation
 29 factor.

30 Based on the Lagrange equation and duality theory, the optimization problem can be converted into a dual problem:

$$31 \quad L(W, b, \xi, \alpha) = \frac{1}{2} W^T W + \frac{C}{2} \sum_{j=1}^n \xi_j^2 - \sum_{j=1}^n \alpha_j (W^T \varphi(x_j) + b + \xi_j - y_j) \quad (8)$$



1 where α_j is the Lagrange multiplier.

2 The solution of the optimization equation is obtained by solving the partial differential form of the Lagrange equation with
 3 respect to W , b , ξ_j , α_j . The optimization equations are expressed as follows.

$$4 \quad \begin{cases} \frac{\partial L}{\partial W} = 0 \Rightarrow W = \sum_{j=1}^n \alpha_j y_j \varphi(x_j) \\ \frac{\partial L}{\partial b} = 0 \Rightarrow \sum_{j=1}^n \alpha_j y_j = 0 \\ \frac{\partial L}{\partial \xi_j} = 0 \Rightarrow \alpha_j = C \xi_j \\ \frac{\partial L}{\partial \alpha_j} = 0 \Rightarrow y_j [W^T \varphi(x_j) + b] - 1 + \xi_j \end{cases} \quad (9)$$

5 The linear equations can be obtained by solving Eq. (9) with the elimination of W and ξ :

$$6 \quad \begin{bmatrix} 0 & I^T \\ I & ZZ^T + C^{-1}E \end{bmatrix} \begin{bmatrix} b \\ \alpha \end{bmatrix} = \begin{bmatrix} 0 \\ y \end{bmatrix} \quad (10)$$

7 where $y = [y_1, y_2, \dots, y_l]^T$, $I = [1, \dots, 1]^T$, $\alpha = [\alpha_1, \alpha_2, \dots, \alpha_l]^T$, $Z = [\varphi(x_1), \varphi(x_2), \dots, \varphi(x_l)]^T$ and E is the unit
 8 matrix with l dimensions.

9 Then, the regression prediction model of the LSSVM can be rewritten based on the above optimization problem:

$$10 \quad f(x) = \sum_{j=1}^n \alpha_j K(x, x_j) + b \quad (11)$$

11 where $K(x_j, x)$ is a kernel function.

12 In the paper, we select the radial basis kernel function as the kernel function in the LSSVM model to obtain the optimal
 13 solutions due to its strong nonlinear mapping ability and wide convergence domain (Min and Lee 2005; Altunel et al. 2015; Elbisy
 14 2015; Farzan et al. 2015):

$$15 \quad K(x_j, x) = \exp(-(x - x_j)^2) / (2\sigma) \quad (12)$$

16 where σ is a parameter of the kernel function.

17 The parameter of the model C and the parameter of the kernel function σ significantly influence the prediction
 18 performance. The parameter C represents the error tolerance. The more accurate the parameter is, the higher the prediction
 19 performance is, but this can lead to overtraining. The parameter σ implicitly determines the spatial distribution of data mapping
 20 in the new feature space. Therefore, some measures should be taken to optimize the LSSVM parameters.

21 2.3 GA

22 Currently, several intelligent algorithms are used to solve optimization problem, such as the GA (Li et al. 2010; Ali et al.
 23 2013), grid algorithm (Lin 2001), particle swarm optimization (Vandenbergh and Engelbercht 2006) and genetic programming
 24 (Garg and Tai 2011; Shen et al. 2012). However, compared with the GA, the grid algorithm is tedious and cannot yield
 25 satisfactory results (Gu et al. 2011). For discrete optimization problems, particle swarm optimization performs poorly and often
 26 yields local optima (Fei et al. 2009). In addition, genetic programming, which was developed by Koza (1992), provides solutions
 27 to complex problems using evolutionary algorithms, and the method is typically expressed as a tree structure that consists of
 28 terminals and functions; however, it is difficult to generate new individuals, which seriously affects the convergence rate (Garg et

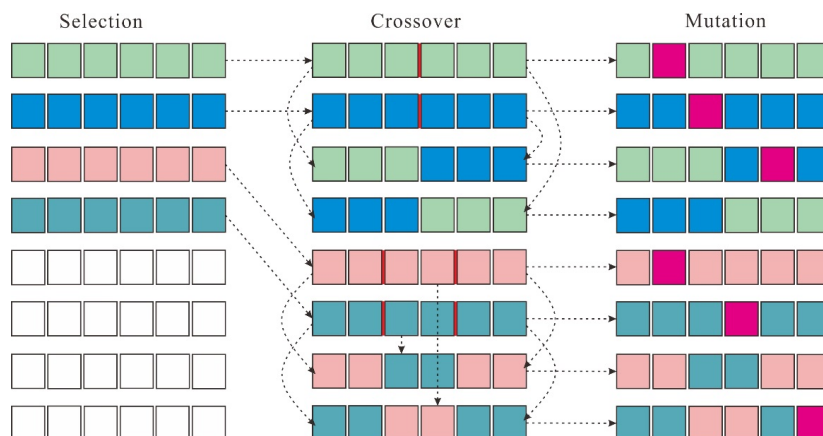


1 al. 2014). In this paper, we select the GA to determine the best parameters (C and σ) of the LSSVM for predicting landslide
2 displacement.

3 The GA is a computational model that simulates natural selection and the biological evolution processes of genetic
4 mechanisms. The GA provides solutions for complicated problems using evolutionary algorithms (Levasseur et al. 2008; Hejazi et
5 al. 2013). The typical genetic operations include selection, crossover and mutation.

6 Based on certain methods and theories, selection operations, such as the fitness-ratio selection algorithm, ranking algorithm,
7 Monte Carlo selection and tournament selection, are commonly used to choose a parental generation from a population based on
8 an individual's fitness value. Crossover operation can generate two new offspring by selecting random codes from two parents
9 and then exchanging their respective branches. Point mutation is commonly used as the mutation operator. By selecting a random
10 node from a parent, a new individual is generated by substituting the selected random node into another parent branch. A typical
11 genetic algorithm is shown in Fig. 1. Selection operations, crossover operations and mutation operations are probabilistic, and
12 with a probability of over 90%, crossover operations are the most widely used.

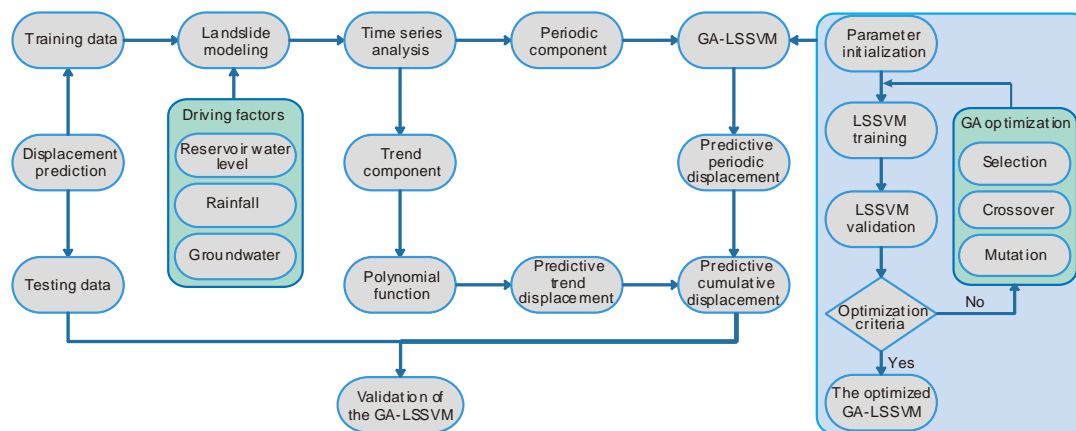
13 By randomly choosing selection, crossover and mutation operations and beginning with any initial population, a set of new
14 individuals with better fitness can be produced. Therefore, the GA will terminate when the fitness of an optimal individual reaches
15 the threshold value, the fitness of an optimal individual and the fitness of the population no longer increase, or the number of
16 iterations reaches the default threshold.



17
18 Fig. 1 Diagram of genetic operations

19 **2.4 GA-LSSVM model**

20 To obtain the best model, the parameters of the model must be carefully selected in advance (Duan et al. 2003). According
21 to some research results (Lessmann et al. 2005; Pourbasheer et al. 2009), the GA has the advantages of reducing the blindness of
22 artificial selection and enhancing the discrimination ability of the LSSVM model. Modeling with this method can achieve high
23 precision if the training samples are reliable. The sampling data used for landslide displacement prediction are continuous and
24 mutually dependent landslide data applicable for a specific method; thus, the data are essentially independent sampling data.
25 In this paper, the periodic component displacement is predicted by the GA-LSSVM model, which has higher accuracy than other
26 models due to the consideration of the trigger factors. MATLAB software is used to execute the model. The flowchart of the
27 GA-LSSVM model is presented in Fig. 2.



1
 2 Fig. 2 The basic flowchart of the GA-LSSVM model, including the establishment of the GA-LSSVM model and the validation of
 3 the model

4 **3 Case study: Shuping landslide**

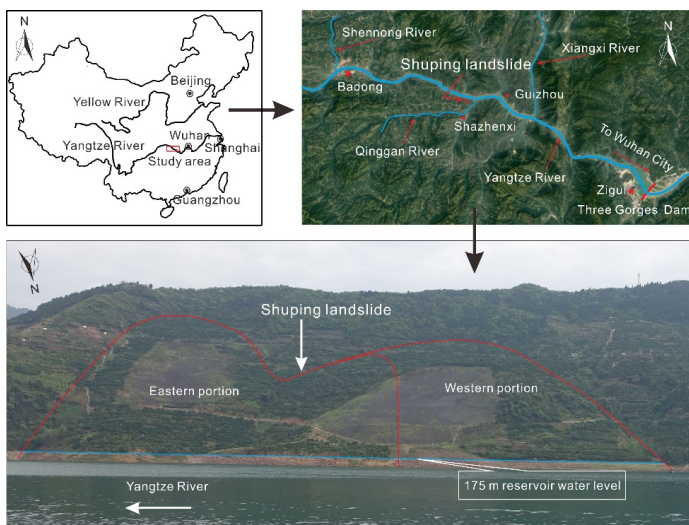
5 **3.1 Geological conditions**

6 The Shuping landslide is located in Shazhenxi town, Zigui country, Hubei province, China, near the Yangtze River and
 7 approximately 47 km into the upper reach of Three Gorges Dam (Fig. 3). The sliding direction of Shuping landslide is N11°E, and
 8 the landslide presents a sector in a topographic map (Fig. 3). The reservoir water level in Fig. 3 is 166 m. The topography is
 9 relatively flat, with a mean slope angle of 22°. The highest elevation of the landslide is 400 m above sea level. The head scarp of
 10 the landslide reaches to the riverbed of the Yangtze River at 60 m in elevation. The landslide covers an area of approximately $54 \times$
 11 10^4 m^2 , with an average length of 800 m in the longitudinal direction and an average length of 670 m in the transverse direction.
 12 The landslide volume is $2070 \times 10^4 \text{ m}^3$, with an average sliding surface depth of 40 m (Fig. 4). Fig. 4 shows the eight GPS
 13 monitoring stations installed on the ground surface of the landslide, as well as four inclinometer monitoring holes. The bedrock is
 14 mainly sandy mudstone. The strata comprise the Triassic Badong formation. The dip direction of the bedrock is between 120° and
 15 165°, and the dip angle is between 10° and 35°. The landslide is divided into an eastern portion and a western portion, and the
 16 materials of the landslide mainly include Quaternary deposits and soils containing silty clay and rock fragments with a loose and
 17 disorderly structure (Fig. 5). Fig. 5 shows a longitudinal section of the eastern portion. The sliding surface is steep in the upper
 18 area, which is located between the deposits and the bedrock.

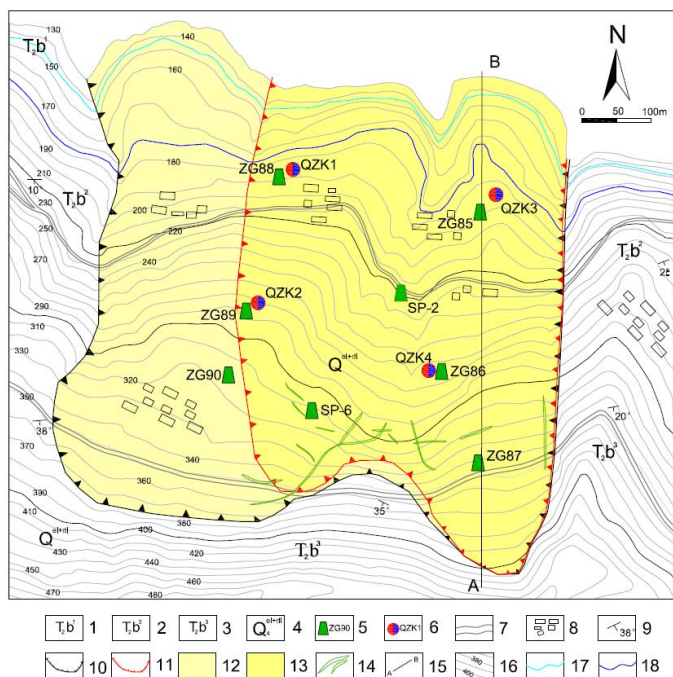
19 Underground moisture beneath the landslide is primarily pore water flowing through a loose medium that consists of
 20 colluviums, deposits, etc. After the water storage began in Three Gorges Reservoir in June 2003, the landslide deformation
 21 became more active. Various external factors affect the landslide displacement, including rainfall, the reservoir water level, surface
 22 water infiltration, groundwater, etc.

23 **3.2 Monitoring data and deformation characteristics of the landslide**

24 Field investigations revealed that there was no obvious deformation of this landslide before the first impoundment of the
 25 reservoir on June 15, 2003. However, macroscopic cracks occurred in the landslide, including through roads and houses, after the
 26 first impoundment. To measure the deformation characteristics and stability of the landslide, monitoring stations were built to
 27 observe the interactions between different portions of the landslide. The monitoring methods include geodetic surveys, drilling,
 28 meteorological observations and geological investigations. Thus, the development processes and evolution of the landslide can be
 29 analyzed qualitatively using monitoring data from eight monitoring stations and four inclinometer monitoring holes located along
 30 the longitudinal direction of the landslide (ZG85 to ZG90, SP-2 and SP-6, QZK1 to QZK4 in Fig. 4).



1
 2 Fig. 3 Location of the study area and panorama of the Shuping landslide and landslide subzones



3
 4 Fig. 4 Geology and deformation monitoring map of Shuping landslide

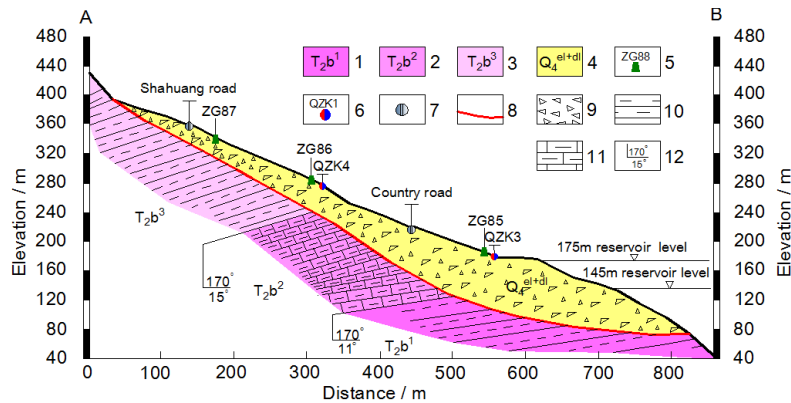
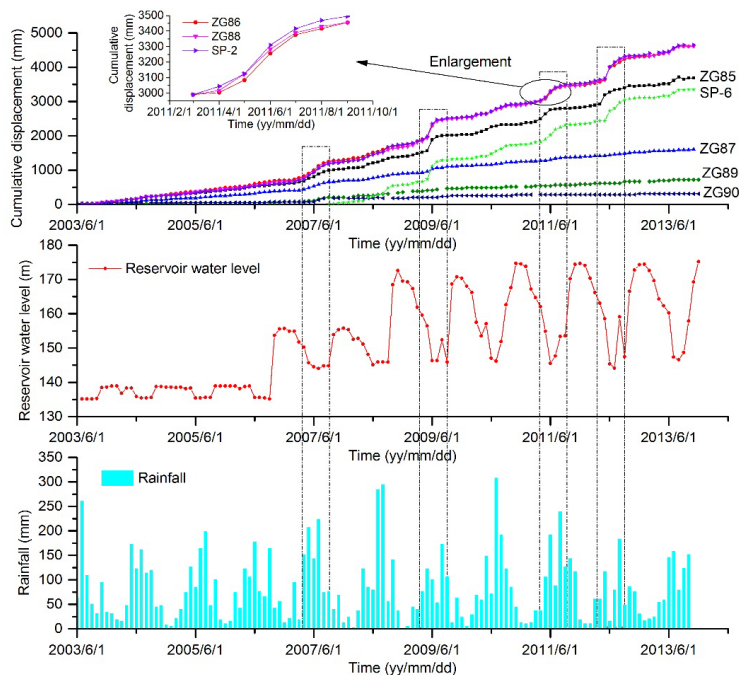


Fig. 5 Geological longitudinal section (line A-B in Fig. 4) of Shuping landslide

1
 2
 3
 4
 5
 6
 7
 8
 9
 10
 11
 12
 13
 14
 15
 16
 17
 18

Fig. 6 shows the monitoring results between July 2003 and October 2013, including rainfall and reservoir water level, which exhibit near step-like characteristics after the first impoundment. The displacements in the middle (ZG86) and head scarp (ZG85) areas were greater than that in the back scarp (ZG87) area of longitudinal section A-B, and the displacements in the head scarp (ZG88) and middle (ZG89) areas were greater than that in the back scarp (ZG90) area in the western zone. These observations suggest that the displacement of landslide increased steadily, and Shuping landslide displayed retrograde style deformation from the lower part to the upper part. The cumulative displacements at the monitoring stations located in the frontal areas were relatively low, with an average value of 880 mm, and the cumulative displacements at the monitoring stations located in the middle-rear areas were very high, with an average value of 3890 mm. Overall, landslide deformation in the eastern zone was greater than that in the western zone. Based on the reservoir water level data and the displacements measured at eight monitoring stations, the cumulative displacement rate increased after the initial impoundment. Due to the increased rainfall and decreased reservoir water level between April and August each year, the cumulative displacement rises rapidly. Notable leap characteristics can be observed in 2007, 2009, 2011 and 2012. The variations in reservoir water level and heavy rainfall reduced the matric suction and the shear strength of soils and rocks. In addition, the uplift pressure, hydrostatic pressure and hydrodynamic pressure acting on the landslide changed periodically. As a result, landslide deformation increased and the stability of the landslide decreased.



1

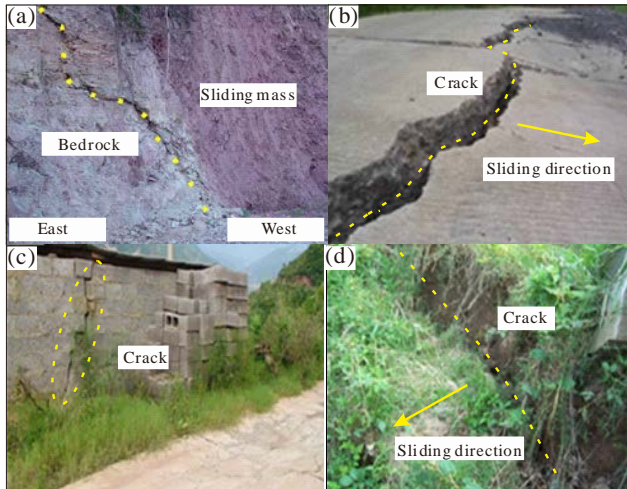
2 Fig. 6 The relationships between rainfall, reservoir water level and displacement

3 Many deformation or failure phenomena were observed in the Shuping landslide. These phenomena increase the risk of
4 endangering the lives of local inhabitants, as well as local property and infrastructure. In June 2003, a crack was generated in the
5 middle part of the landslide on the outside of a local road, as shown in Fig. 7(a). In 2006, the reservoir water level increased to
6 156 m for the first time. Fig. 7(b) shows that the crack gradually extended to a width of 10 cm within 3 months after finishing the
7 road in April 2007. In August 2008, after a heavy storm occurred, deformation and tension cracks developed in the eastern portion
8 of the landslide and affected houses, as shown in Fig. 7(c). Since 2009, the reservoir water level has increased gradually to 175 m.
9 In June 2009, the western portion of the landslide started cracking, with a maximum crack width of 20 cm and depth of 20-50 cm.
10 In addition, several tension cracks formed at the eastern landslide boundary. The tension cracks in the eastern portion are shown in
11 Fig. 7(d). In recent years, the cumulative deformation rate has remained low due to the relatively stable reservoir water level,
12 which has fluctuated between 145 m and 175 m.

13 Therefore, the macroscopic deformation characteristics suggest that deformation in the western portion of the landslide is
14 smaller than that in the eastern portion, and the Shuping landslide is affected by reservoir water level fluctuations and rainfall.
15 When rainfall increases abruptly and the reservoir water level drops between April and August annually, the landslide becomes
16 active, which increases landslide deformation. In other conditions, the landslide undergoes slow deformation at a constant speed.

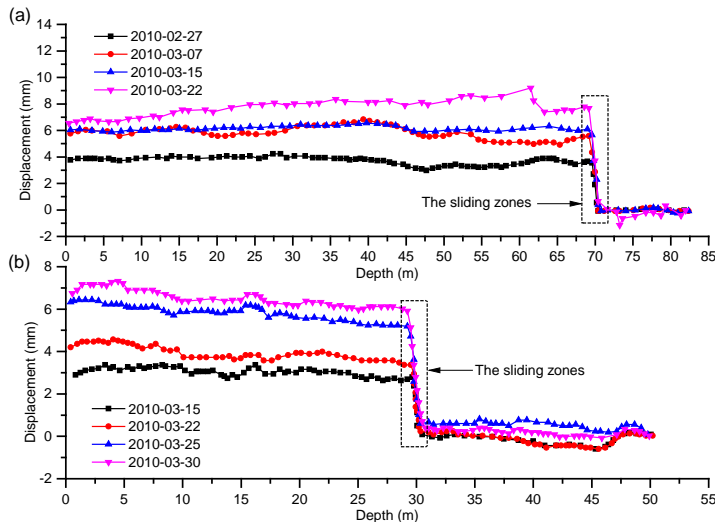
17 In addition, groundwater, which is regarded as an active geologic agent, is one of the main factors that induces landslide
18 instability. In the rising phase of reservoir water level, the groundwater level gradually increases, with a slight lag behind the
19 increase in the reservoir water level. Conversely, the groundwater level decreases in the declining phase of the reservoir water
20 level. Moreover, the uplift pressure and seepage force of groundwater are dynamic processes that affect landslide stability.
21 Therefore, groundwater influences cumulative displacement.

22 Overall, the reservoir water level, rainfall and groundwater are the major factors that influence the cumulative displacement
23 of the Shuping landslide. The landslide displacement obviously increases when the reservoir water level decreases or when
24 rainfall is heavy and continuous because the materials in the sliding mass are degraded by the excess moisture and the additional
25 hydrodynamic pressure.



1
 2 Fig. 7 Photographs of the ground cracks in the landslide (Ren et al., 2015): (a) crack in the middle of the landslide on the outside
 3 of the local road, (b) failure state of the local road, (c) wall cracking and subsidence in the eastern portion, and (d) the tension
 4 cracks in the eastern portion

5
 6 Several years of monitoring data show that the landslide deformation differences are manifested in the ground surface, and
 7 they display vertically distributed characteristics with elevation. In conclusion, the surface displacements below 200 m in
 8 elevation are larger than those above 200 m, and deformation is largest close to 175 m, which is the upper limit of the reservoir
 9 water level. This observation is due to the considerable influence of fluctuations in the reservoir water level on the landslide area
 10 below 200 m. The deep deformation of the landslide exhibited distinct differences at different depths, as shown in Fig. 8.
 11 Inclinometer monitoring holes QZK3 and QZK4, QZK1 and QZK2, which are located in the western portion of the landslide,
 12 exhibited small deformation and similar deformation trends. Thus, their lateral displacement curves are not presented, and only the
 13 curves of QZK3 and QZK4 are illustrated in this paper. The figures show that the sliding zones of QZK3 and QZK4 are located at
 14 elevations of 70 m and 30 m, respectively. Furthermore, the displacement change in the shallow sliding zones of both QZK3 and
 15 QZK4 is larger than that in the deep sliding zone.



16
 17 Fig. 8 Lateral displacements of Shuping landslide: (a) inclinometer monitoring hole QZK3 and (b) inclinometer monitoring hole



1 QZK4

2 **4 Landslide displacement prediction**

3 Based on the analysis of the deformation characteristics of Shuping landslide and the GA-LSSVM model above and due to
 4 the obvious nonlinear and step-like deformation characteristics of monitoring stations ZG85, ZG86 and ZG87, we select only
 5 these stations along longitudinal section A-B to verify and establish the prediction model. The model includes information
 6 regarding rainfall, the reservoir water level, human activities and the long-term behavior of Shuping landslide. Because the
 7 integrity of the data collected at monitoring points has an effect on the displacement prediction, the monitoring data from July
 8 2003 to October 2013 are selected to explore landslide deformation. The data before October 2012 are used to train the
 9 GA-LSSVM model, and the data after October 2012 are used to test the model.

10 **4.1 Prediction of the trend component displacement**

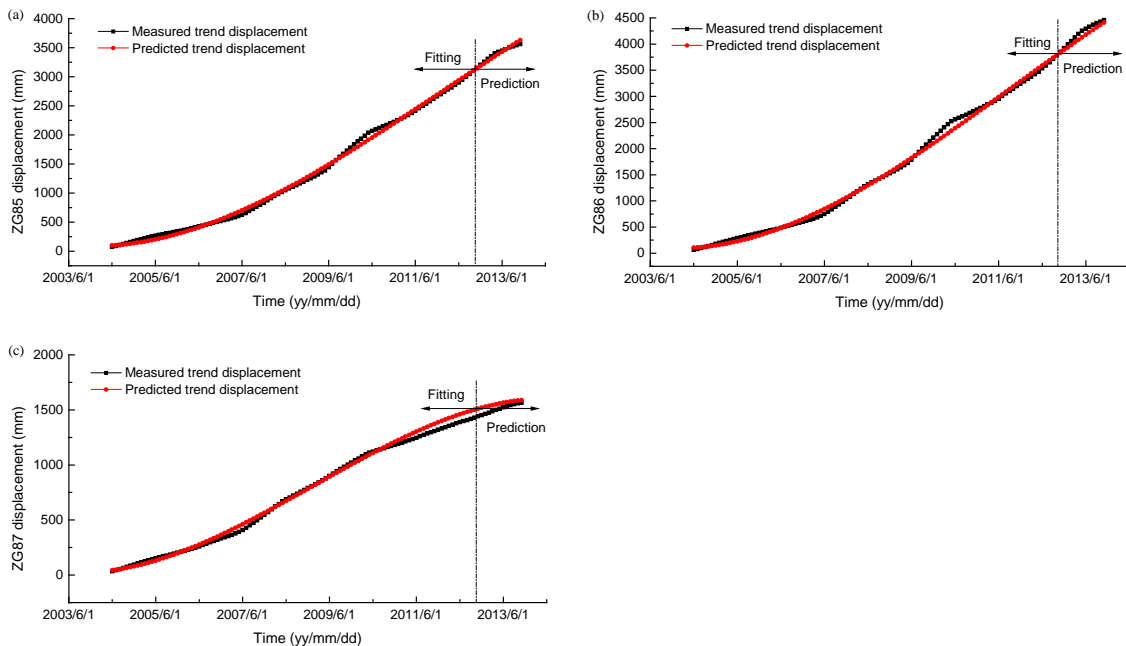
11 Due to the scheduling period of the reservoir and the rainfall cycle, we choose 12 months as the moving average period.
 12 Because the curves of the trend component displacement versus time have quasi-linear and incremental characteristics, we use
 13 polynomial functions to fit these curves and provide the best-fitted results. The predicted and measured results of the trend
 14 component displacement at monitoring stations ZG85, ZG86 and ZG87 are shown in Figs. 9(a), 9(b) and 9(c), respectively. They
 15 indicate that the polynomial function provides good prediction performance for the trend component displacement and the fitted
 16 functions are expressed in Eqs. (13), (14) and (15).

17
$$p_t = -0.0015t^3 + 0.4744t^2 - 8.4975t + 128.83 \quad R^2=0.9980 \quad (13)$$

18
$$p_t = -0.002t^3 + 0.604t^2 - 10.468t + 143.35 \quad R^2=0.9978 \quad (14)$$

19
$$p_t = -0.0015t^3 + 0.3088t^2 - 2.7227t + 29.832 \quad R^2=0.9976 \quad (15)$$

20



21

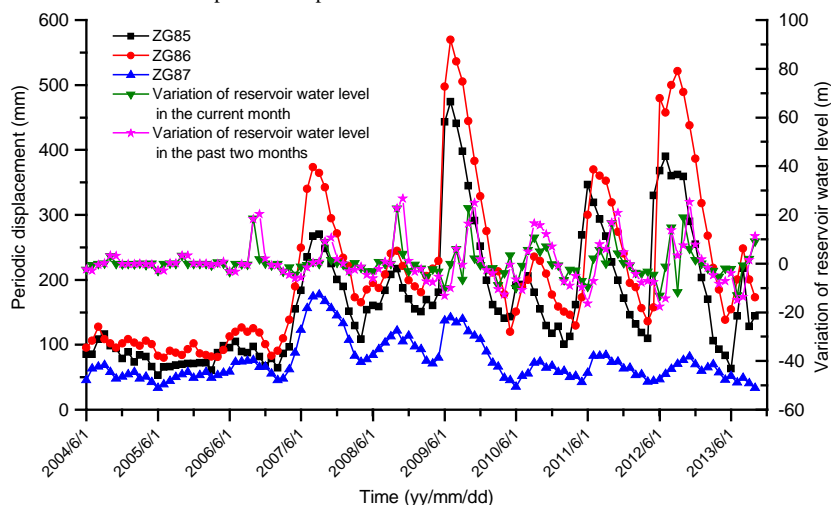
22 Fig. 9 Measured and predicted trend component displacement of Shuping landslide

23 **4.2 The predicted periodic component displacement**

24 The periodic component displacement is determined by subtracting the extracted trend component displacement from the
 25 cumulative displacement. The periodic displacement and the major influencing factors are illustrated in Figs. 10 and 11. The



1 variations in the periodic displacement are consistent with those in the influencing factors. The reservoir water level, rainfall and
 2 groundwater considerably influence the periodic displacement. For example, large periodic displacement can be observed in July
 3 2009 and September 2012 when the landslide was affected by heavy rainfall and large variations in reservoir water level.
 4 Although the variation in reservoir water level was small before April 2007, the periodic displacement still exhibited small
 5 fluctuations due to the effects of rainfall and groundwater. After April 2007, several obvious peaks can be observed in the periodic
 6 displacement-time curves during periods of decreasing reservoir water level. For example, the periodic displacement increased
 7 from May to July 2009 and from May to September 2012. However, when the reservoir water level increased from 145 m to 175
 8 m, the periodic displacement gradually decreased. The main reason for the above conditions was that the increase in the reservoir
 9 water level increased the pressure on the surface of the landslide, thereby increasing the resistance force. Conversely, the sliding
 10 force increased when the reservoir water level decreased. The periodicity of the rainfall also affected the periodic displacement.
 11 The periodic displacement increased with increasing rainfall and reached a peak value in summer, which reflects a certain lag.
 12 Groundwater depth was measured at the head scarp of the landslide at an elevation of 181 m in inclinometer monitoring hole
 13 QZK3. The change in groundwater depth exhibits considerable agreement with rainfall and reservoir water level fluctuations, with
 14 a slight lag observed for the latter. Due to the slight lag with the reservoir water level, groundwater increased the hydrodynamic
 15 pressure during periods when the reservoir water level decreased or remained stable, which resulted in continuous deformation of
 16 the landslide. Therefore, in the shallow groundwater zone, the periodic displacements measured at the three monitoring stations
 17 exhibited considerable fluctuations. In conclusion, the results in Figs. 10 and 11 show that the reservoir water level is the factor
 18 that most influences the periodic displacement.



19

20 Fig. 10 The relationship between reservoir water level and the periodic displacement at GPS monitoring stations

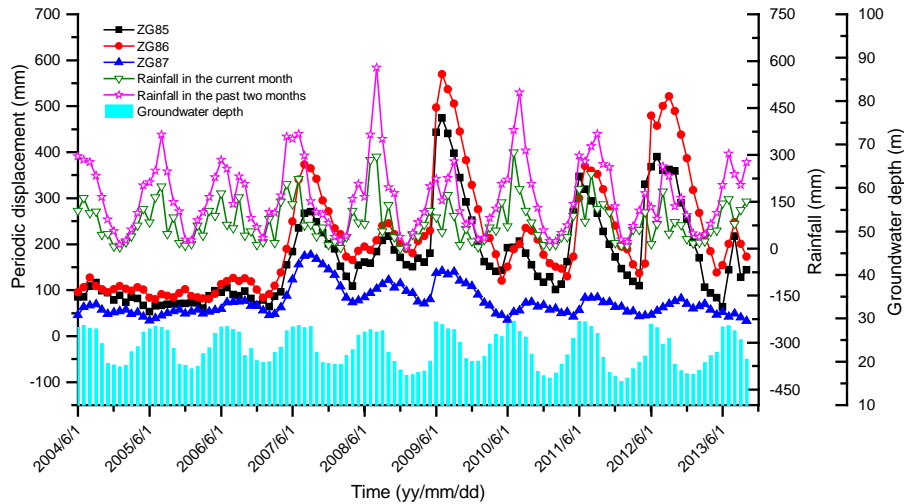


Fig. 11 The relationships between rainfall, groundwater depth and periodic displacement at GPS monitoring stations

The grey relational grade can represent the proximity degree between two series. If the trends in the two series are consistent or the degree of synchronous change is high, then the relational grade associated with system development is large. Otherwise, the relational grade is small. To remove the influence of dimensional data, data series must be normalized before calculating the relational grades, including the series of periodic displacement, rainfall and reservoir water level changes. The normalized formula can be expressed by Eq. (16):

$$\bar{y} = \frac{y - y_{\min}}{y_{\max} - y_{\min}} \quad (16)$$

where \bar{y} is the normalized value, y is the original value, y_{\max} is the maximum value of the data series, and y_{\min} is the minimum value of the data series.

Based on the grey relational analysis method, distinguishing coefficient is 0.5, and the relational grades between the influencing factors and the periodic displacements are shown in Table 1. We can use the large grey relational grades as the input variables in the GA-LSSVM model. When the relational grade is larger than 0.6, the influencing factor is closely correlated with the periodic displacement, which suggests that the selection of the influencing factor for predicting periodic displacement is reasonable (Wang 2003; Wang et al. 2004). Therefore, considering the characteristics of the periodic displacement and the relational grades between variables, the cumulative rainfall in the current month, the cumulative rainfall in the past two months, the reservoir water level, the variation in the reservoir water level in the current month, the variation in the reservoir water level in the past two months, and groundwater depth are selected as input variables. Moreover, the periodic component displacement is established as the output variable for use in the GA-LSSVM model.

Table 1 Relational grades between input variables and the periodic displacements

Monitoring station	Relational grade					
	The cumulative rainfall in the current month	The cumulative rainfall in the past two months	The reservoir water level	The variation of The reservoir water level in the current month	The variation of The reservoir water level in the past two months	Groundwater depth
ZG85	0.700	0.705	0.763	0.797	0.768	0.718
ZG86	0.682	0.691	0.756	0.794	0.770	0.714
ZG87	0.692	0.705	0.724	0.794	0.780	0.720

The parameters of the LSSVM are optimized by the GA, including the best values of C and σ . Table 2 shows the optimal

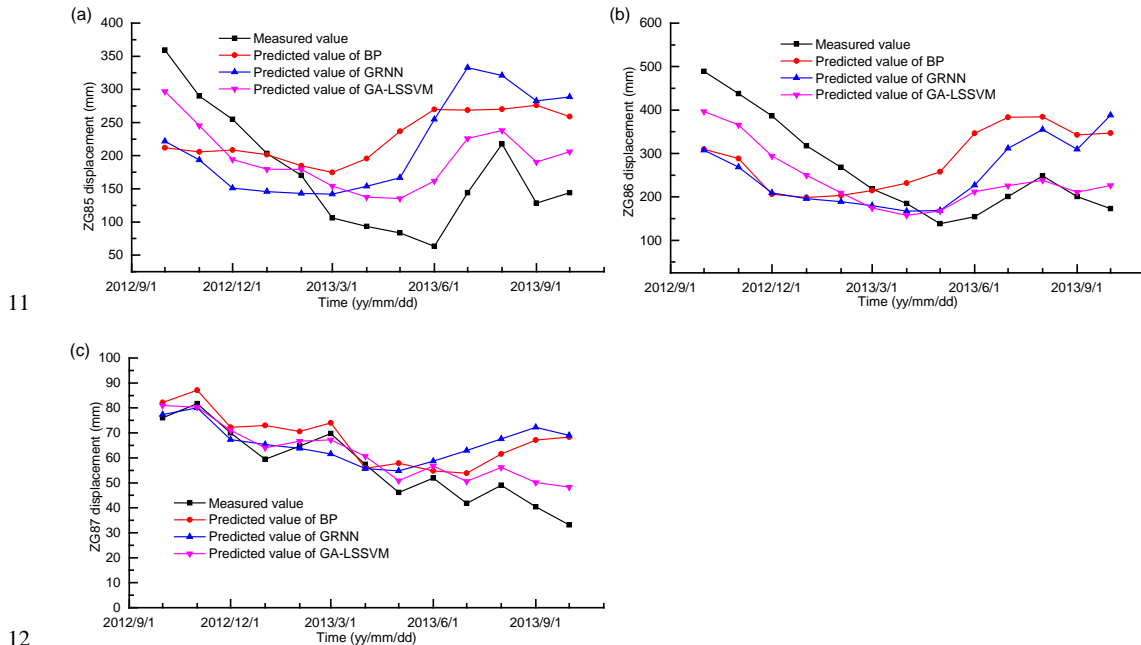


1 parameters of the LSSVM. The maximum generation threshold of the GA is 200, and the population number is 20. To validate the
 2 prediction ability of the GA-LSSVM model, we compare the results of generalized regression neural network (GRNN) and back
 3 propagation (BP) with two hidden layers with the result of the GA-LSSVM model. In this paper, the smoothing factor of the
 4 GRNN is 0.48, and there are 10 nodes in one of the hidden layers and 11 nodes in the other hidden layer of the BP.

5 Table 2 Optimal parameters of the LSSVM model

Number	Monitoring station	C	σ
1	ZG85	11.8234	6.4122
2	ZG86	4.7346	8.0545
3	ZG87	39.7819	5.7981

6 The prediction results of the periodic component displacement are shown in Fig. 12. The predicted values of the three
 7 prediction models and the measured values are consistent and illustrate similar trends. However, the predicted values obtained
 8 using the GA-LSSVM exhibit better agreement with observations than do those of the other methods. Notably, the advantages of
 9 the model are clear from April 2013 to October 2013, as the periodic component displacement exhibited good agreement with the
 10 major influencing factors during a period of heavy rainfall and large fluctuations in the reservoir water level.



11
 12
 13 Fig. 12 Measured displacement and predicted periodic displacement of Shuping landslide

14 **4.3 Predicted cumulative displacement**

15 The predicted cumulative displacement is determined from the sum of the predicted trend displacement and the predicted
 16 periodic displacement. The predicted cumulative displacements and the measured values are presented in Table 3, Table 4 and
 17 Table 5 for monitoring station ZG85, ZG86 and ZG87, respectively. The results given in Table 3, Table 4 and Table 5 suggest that
 18 the GA-LSSVM model has better prediction performance than the GRNN model and the BP model, with a smaller relative error.
 19 Comparisons between the predicted values of cumulative displacement and measured values are shown in Fig. 13. The diagonal
 20 line shows the best prediction result in Fig. 13. The results are underestimated if the predicted values are located below the
 21 diagonal line, whereas the predicted values located above the line are overestimated. The predicted values from all the monitoring
 22 stations show good consistency with the measured values, as shown in Fig. 13.

23 Table 3 Comparison between the predicted values of cumulative displacement and measured values at monitoring station ZG85

Time	Measured	GA-LSSVM	GRNN	BP
------	----------	----------	------	----



	value (mm)	Predicted value (mm)	Relative error (%)	Predicted value (mm)	Relative error (%)	Predicted value (mm)	Relative error (%)
2012/10/1	3460.208	3399.937	1.74	3324.829	3.91	3315.157	4.38
2012/11/1	3442.907	3389.608	1.55	3337.861	3.05	3349.827	2.78
2012/12/1	3460.208	3379.418	2.33	3336.503	3.58	3393.732	1.96
2013/1/1	3460.208	3406.014	1.57	3371.989	2.55	3427.727	0.95
2013/2/1	3477.509	3446.374	0.90	3410.133	1.94	3452.011	0.74
2013/3/1	3460.208	3462.169	0.06	3449.721	0.30	3482.668	0.64
2013/4/1	3494.81	3485.798	0.26	3502.356	0.22	3543.963	1.39
2013/5/1	3512.111	3524.423	0.35	3555.754	1.24	3625.738	3.13
2013/6/1	3512.111	3591.262	2.25	3684.274	4.90	3699.022	5.05
2013/7/1	3615.917	3695.444	2.20	3802.473	5.16	3738.225	3.27
2013/8/1	3719.723	3747.513	0.75	3830.496	2.98	3779.618	1.58
2013/9/1	3650.519	3740.002	2.45	3832.151	4.98	3825.664	4.58
2013/10/1	3685.121	3795.259	2.99	3877.587	5.22	3848.299	4.24

1 Table 4 Comparison between the predicted values of cumulative displacement and measured values at monitoring station ZG86

Time	Measured value (mm)	GA-LSSVM		GRNN		BP	
		Predicted value (mm)	Relative error (%)	Predicted value (mm)	Relative error (%)	Predicted value (mm)	Relative error (%)
2012/10/1	4273.356	4183.984	2.09	4094.396	4.19	4096.849	4.13
2012/11/1	4290.657	4201.857	2.07	4104.93	4.33	4124.839	3.86
2012/12/1	4307.958	4149.796	3.67	4094.607	4.95	4091.602	5.02
2013/1/1	4307.958	4164.444	3.33	4130.77	4.11	4133.425	4.05
2013/2/1	4325.26	4192.775	3.06	4172.182	3.54	4186.816	3.20
2013/3/1	4342.561	4256.46	1.98	4212.082	3.00	4246.771	2.21
2013/4/1	4377.163	4317.892	1.35	4247.617	2.96	4312.109	1.49
2013/5/1	4394.464	4326.232	1.55	4297.626	2.20	4386.529	0.18
2013/6/1	4446.367	4388.693	1.30	4403.464	0.96	4523.094	1.73
2013/7/1	4532.872	4495.404	0.83	4535.948	0.07	4607.573	1.65
2013/8/1	4619.377	4609.902	0.21	4626.647	0.16	4656.543	0.80
2013/9/1	4602.076	4579.721	0.49	4628.676	0.58	4661.733	1.30
2013/10/1	4602.076	4592.204	0.21	4754.15	3.30	4713.128	2.41

2 Table 5 Comparison between the predicted values of cumulative displacement and measured values at monitoring station ZG87

Time	Measured value (mm)	GA-LSSVM		GRNN		BP	
		Predicted value (mm)	Relative error (%)	Predicted value (mm)	Relative error (%)	Predicted value (mm)	Relative error (%)
2012/10/1	1505.19	1561.869	3.77	1578.221	4.85	1583.026	5.17
2012/11/1	1522.491	1580.602	3.82	1590.364	4.46	1597.352	4.92
2012/12/1	1522.491	1580.359	3.80	1586.605	4.21	1591.506	4.53
2013/1/1	1522.491	1581.923	3.90	1593.249	4.65	1600.855	5.15
2013/2/1	1539.792	1585.652	2.98	1599.822	3.90	1606.609	4.34
2013/3/1	1557.093	1600.959	2.82	1605.274	3.09	1617.769	3.90
2013/4/1	1557.093	1601.648	2.86	1606.713	3.19	1606.812	3.19
2013/5/1	1557.093	1608.744	3.32	1612.571	3.56	1615.702	3.76
2013/6/1	1574.394	1620.881	2.95	1622.897	3.08	1618.934	2.83
2013/7/1	1574.394	1620.703	2.94	1632.984	3.72	1623.904	3.14



2013/8/1	1591.696	1631.651	2.51	1643.08	3.23	1637.051	2.85
2013/9/1	1591.696	1630.511	2.44	1652.604	3.83	1647.566	3.51
2013/10/1	1591.696	1633.119	2.60	1653.808	3.90	1653.139	3.86

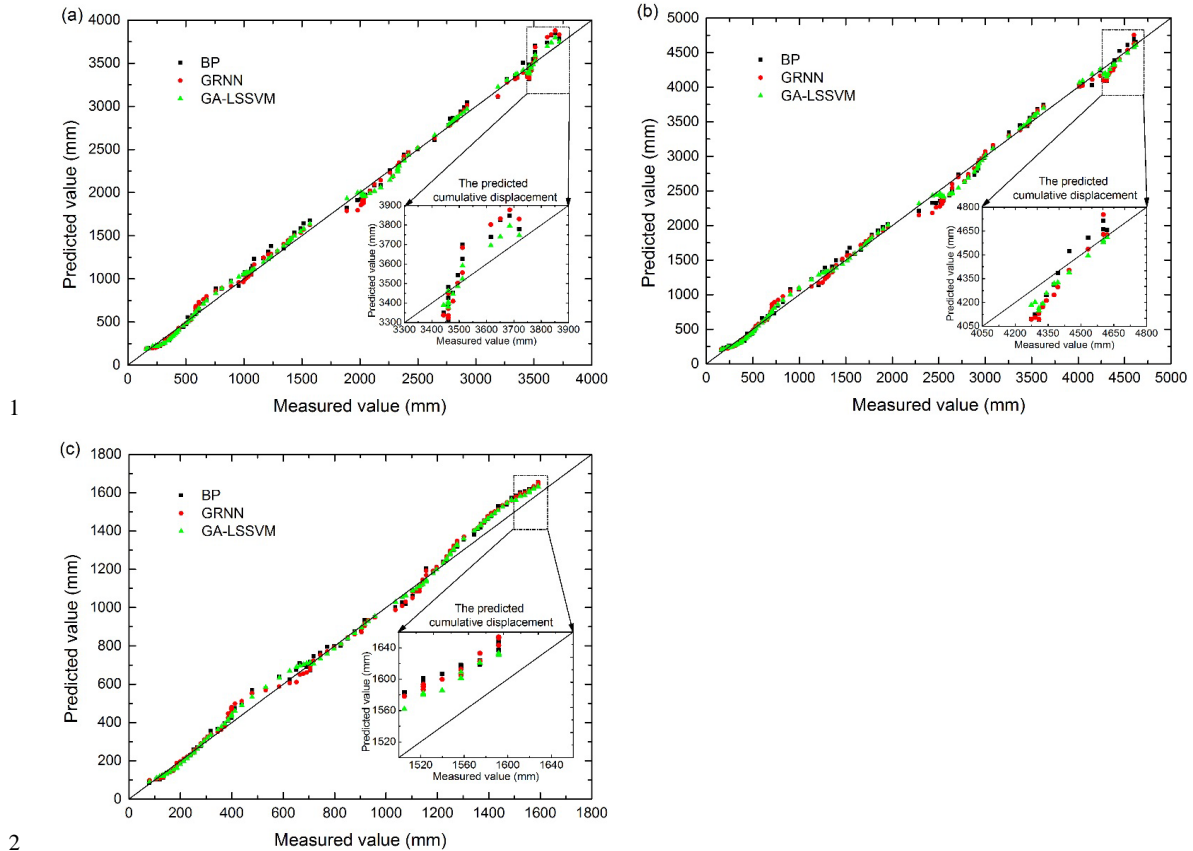


Fig. 13 Measured values versus predicted values of the cumulative displacement: (a) monitoring station ZG85, (b) monitoring station ZG86, and (c) monitoring station ZG87

5 Verification and error analyses

Three loss functions are used to assess the prediction performance and accuracy of the proposed model: the root mean square error (*RMSE*), mean absolute error (*MAE*), and mean absolute percentage error (*MAPE*). Then, the optimal parameters with minimum error are used to train the LSSVM model. The *RMSE*, *MAE* and *MAPE* formulas are as follows:

$$RMSE = \sqrt{\frac{1}{n} \sum_{i=1}^n (s_i - s_i^*)^2} \quad (17)$$

$$MAE = \frac{1}{n} \sum_{i=1}^n |s_i - s_i^*| \quad (18)$$

$$MAPE = \frac{1}{n} \sum_{i=1}^n \left| \frac{s_i - s_i^*}{s_i} \right| \quad (19)$$

where s_i is the measured value, s_i^* is the predicted value, and n is the number of predicted values.



1 The performances of different models for landslide displacement prediction are assessed based on the *RMSE*, *MAE* and
 2 *MAPE*, as presented in Table 6. The prediction precision of the GA-LSSVM model based on time series analysis is better than that
 3 of the GRNN and the BP. Notably, the *RMSE*, *MAE* and *MAPE* values of the GA-LSSVM model were 63.4076, 56.6098 and
 4 1.587% lower than those of the GRNN model, respectively, and 49.3696, 43.5537 and 1.225% lower than those of the BP model
 5 for monitoring station ZG85. The predicted results for monitoring stations ZG86 and ZG87 exhibited similar trends. According to
 6 the prediction results, the GA-LSSVM model has good deduction ability for landslide displacement prediction and can provide
 7 assistance in early risk assessment and landslide forecasting.

8 Table 6 Comparison of the performance of cumulative displacement prediction for the three models

Model	<i>RMSE</i> (mm)			<i>MAE</i> (mm)			<i>MAPE</i> (%)		
	ZG85	ZG86	ZG87	ZG85	ZG86	ZG87	ZG85	ZG86	ZG87
GA-LSSVM	62.4146	87.7215	49.0485	53.0048	74.0601	48.5392	1.492	1.703	3.131
GRNN	125.8222	134.6764	59.8173	109.6146	115.1067	59.2756	3.079	2.643	3.821
BP	111.7842	123.1948	62.0223	96.5585	107.6724	60.9701	2.717	2.464	3.935

9 **6 Conclusion**

10 Landslide displacement prediction is one of the focuses of landslide research. In this paper, we use the deformation of a
 11 step-like landslide (Shuping landslide) as an example. According to time series analysis, the cumulative displacement is
 12 decomposed into a trend component displacement representing the trend of landslide deformation in the long term and a periodic
 13 component displacement that represents short-term deformation fluctuations. The trend displacement and periodic displacement
 14 are predicted using a polynomial function and the GA-LSSVM model, respectively. The LSSVM yields good fitting results in
 15 predicting the periodic displacement with the GA, which is utilized to determine the optimal parameters of the LSSVM. Based on
 16 our analysis of the deformation of Shuping landslide, the reservoir water level, rainfall and groundwater have major influences on
 17 the cumulative displacement. Therefore, based on the relational grades, we select six influential factors as the input variables. The
 18 predicted cumulative displacement is obtained from the sum of the predicted trend displacement and the predicted periodic
 19 displacement.

20 The GA-LSSVM model displays the highest accuracy, the smallest *RMSE* of 62.4146 mm, the smallest *MAE* of 53.0048
 21 mm, and the smallest *MAPE* of 1.492% at monitoring station ZG85, while these three values are 87.7215 mm, 74.0601 mm and
 22 1.703% at monitoring station ZG86 and 49.0485 mm, 48.5392 mm and 3.131% at monitoring station ZG87. The study results
 23 show that GA-LSSVM provides good performance for landslide displacement prediction, and the GA is appropriate for
 24 determining the optimal parameters used in the LSSVM model. Thus, the GA-LSSVM model can be effectively used to predict
 25 landslide displacement and reflect the corresponding relationships between the major influencing factors and the periodic
 26 component displacement.

27 **Acknowledgments**

28 The authors would like to acknowledge gratefully the Editor and the anonymous reviewers for their constructive criticism
 29 on the earlier version of this paper and offering valuable suggestions that contributed to its improvement. This study was
 30 supported by National Natural Science Foundation of China, Key Project of National Science Foundation of China (No. 41230637,
 31 No. 41502290), the Ministry of Science and Technology of the P. R. China, National Basic Research Program of China (973
 32 Program) (2011CB710600).

33

34 **References**

35 Abdi, M. J., and Giveki, D.: Automatic detection of erythemato-squamous diseases using PSO-SVM based on association rules,
 36 Eng Appl Artif Intel, 26, 603-608, 10.1016/j.engappai.2012.01.017, 2013.
 37 Ahmed, B.: Landslide susceptibility mapping using multi-criteria evaluation techniques in Chittagong Metropolitan Area,
 38 Bangladesh, Landslides, 6, 1077-1095, 10.1007/s10346-014-0521-x, 2013.
 39 Ali Ahmadi, M., Zendejboudi, S., Lohi, A., Elkamel, A., and Chatzis, I.: Reservoir permeability prediction by neural networks
 40 combined with hybrid genetic algorithm and particle swarm optimization, Geophys Prospect, 61, 582-598,
 41 10.1111/j.1365-2478.2012.01080.x, 2013.



- 1 Altinel, B., Can Ganiz, M., and Diri, B.: A corpus-based semantic kernel for text classification by using meaning values of terms,
- 2 Eng Appl Artif Intel, 43, 54-66, 10.1016/j.engappai.2015.03.015, 2015.
- 3 Brockwell, P. J., and Davis, R. A.: Time series: theory and methods, Springer Science & Business Media, 2013.
- 4 Cao, Y., Yin, K., Alexander, D. E., and Zhou, C.: Using an extreme learning machine to predict the displacement of step-like
- 5 landslides in relation to controlling factors, Landslides, 4, 725-736, 10.1007/s10346-015-0596-z, 2016.
- 6 Corominas, J., Moya, J. E., Ledesma, A., Lloret, A., and Gili, J. A.: Prediction of ground displacements and velocities from
- 7 groundwater level changes at the Vallcebre landslide (Eastern Pyrenees, Spain, Landslides, 2, 83-96, 10.1007/s10346-005-0049-1,
- 8 2005.
- 9 Du, J., Yin, K., and Lacasse, S.: Displacement prediction in colluvial landslides, Three Gorges Reservoir, China, Landslides, 10,
- 10 203-218, 10.1007/s10346-012-0326-8, 2013.
- 11 Duan, K., Keerthi, S. S., and Poo, A. N.: Evaluation of simple performance measures for tuning SVM hyperparameters,
- 12 Neurocomputing, 51, 41-59, 10.1016/S0925-2312(02)00601-X, 2013.
- 13 Elbisy, M. S.: Sea wave parameters prediction by support vector machine using a genetic algorithm, J Coastal Res, 314, 892-899,
- 14 10.2112/JCOASTRES-D-13-00087.1, 2015.
- 15 Farzan, A., Mashohor, S., Ramli, A. R., and Mahmud, R.: Boosting diagnosis accuracy of Alzheimer's disease using high
- 16 dimensional recognition of longitudinal brain atrophy patterns, Behav Brain Res, 290, 124-130, 10.1016/j.bbr.2015.04.010, 2015.
- 17 Fei, S., Wang, M., Miao, Y., Tu, J., and Liu, C.: Particle swarm optimization-based support vector machine for forecasting
- 18 dissolved gases content in power transformer oil, Energ Convers Manage, 50, 1604-1609, 10.1016/j.enconman.2009.02.004, 2009.
- 19 Feng, X., Zhao, H., and Li, S.: Modeling non-linear displacement time series of geo-materials using evolutionary support vector
- 20 machines, Int J Rock Mech Min, 41, 1087-1107, 10.1016/j.ijrmm.2004.04.003, 2004.
- 21 Garg, A., and Tai, K.: A hybrid genetic programming-artificial neural network approach for modeling of vibratory finishing
- 22 process, International Proceedings of Computer Science and Information Technology (IPCSIT), 14-19, 2011.
- 23 Garg, A., and Tai, K.: Stepwise approach for the evolution of generalized genetic programming model in prediction of surface
- 24 finish of the turning process, Adv Eng Softw, 78, 16-27, 10.1016/j.advengsoft.2017.01.005, 2014.
- 25 Gelisli, K., Kaya, T., and Babacan, A. E.: Assessing the factor of safety using an artificial neural network: case studies on
- 26 landslides in Giresun, Turkey, Environ Earth Sci, 73, 8639-8646, 10.1007/s12665-015-4027-1, 2015.
- 27 Goetz, J. N., Brenning, A., Petschko, H., and Leopold, P.: Evaluating machine learning and statistical prediction techniques for
- 28 landslide susceptibility modeling, Comput Geosci-Uk, 81, 1-11, 10.1016/j.cageo.2015.04.007, 2015.
- 29 Gu, J., Zhu, M., and Jiang, L.: Housing price forecasting based on genetic algorithm and support vector machine, Expert Syst
- 30 Appl, 38, 3383-3386, 10.1016/j.eswa.2010.08.123, 2011.
- 31 Guzzetti, F., Reichenbach, P., Cardinali, M., Galli, M., and Ardizzone, F.: Probabilistic landslide hazard assessment at the basin
- 32 scale, Geomorphology, 72, 272-299, 10.1016/j.geomorph.2005.06.002, 2005.
- 33 Hejazi, F., Toloue, I., Jaafar, M. S., and Noorzaei, J.: Optimization of earthquake energy dissipation system by genetic algorithm,
- 34 Comput-Aided Civ Infrastruct Eng, 28, 796-810, 10.1111/mice.12047, 2013.
- 35 Hong, H., Pradhan, B., Jebur, M. N., Bui, D. T., Xu, C., and Akgun, A.: Spatial prediction of landslide hazard at the Luxi area
- 36 (China) using support vector machines, Environ Earth Sci, 75, 10.1007/s12665-015-4866-9, 2016.
- 37 Hwang, S., Jeong, M. K., and Yum, B.: Robust relevance vector machine with variational inference for improving virtual
- 38 metrology accuracy, Ieee T Semiconduct M, 27, 83-94, 10.1109/TSM.2013.2286498, 2014.
- 39 Kavzoglu, T., Kutlug Sahin, E., and Colkesen, I.: An assessment of multivariate and bivariate approaches in landslide
- 40 susceptibility mapping: a case study of Duzkoy district, Nat Hazards, 76, 471-496, 10.1007/s11069-014-1506-8, 2015.
- 41 Kawabata, D., and Bandibas, J.: Landslide susceptibility mapping using geological data, a DEM from ASTER images and an
- 42 artificial neural network (ANN), Geomorphology, 113, 97-109, 10.1016/j.geomorph.2009.06.006, 2009.
- 43 Kirschbaum, D. B., Adler, R., Hong, Y., Hill, S., and Lerner-Lam, A.: A global landslide catalog for hazard applications: method,
- 44 results, and limitations, Nat Hazards, 3, 561-575, 10.1007/s11069-009-9401-4, 2010.
- 45 Koza, J. R.: Genetic programming: on the programming of computers by means of natural selection, MIT press, Cambridge, MA,
- 46 1992.



- 1 Lessmann, S., Stahlbock, R., and Crone, S. F.: Optimizing hyperparameters of support vector machines by genetic algorithms, Las
- 2 Vegas, CSREA Press, 2005.
- 3 Levasseur, S., Malécot, Y., Boulon, M., and Flavigny, E.: Soil parameter identification using a genetic algorithm, *Int J Numer Anal*
- 4 *Met*, 32, 189-213, 10.1002/nag.614, 2008.
- 5 Li, F., Tang, B. P., and Liu, W. Y.: Fault diagnosis based on least square support vector machine optimized by genetic algorithm,
- 6 *Journal of Chongqing University*, 33, 14-20, 2010(in Chinese).
- 7 Lian, C., Zeng, Z. G., Yao, W., and Tang, H. M.: Displacement prediction model of landslide based on a modified ensemble
- 8 empirical mode decomposition and extreme learning machine, *Nat Hazards*, 66, 759-771, 10.1007/s11069-012-0517-6, 2013.
- 9 Lian, C., Zeng, Z. G., Yao, W., and Tang, H. M.: Ensemble of extreme learning machine for landslide displacement prediction
- 10 based on time series analysis, *Neural Comput Appl*, 24, 99-107, 10.1007/s00521-013-1446-3, 2014.
- 11 Lian, C., Zeng, Z., Yao, W., and Tang, H.: Multiple neural networks switched prediction for landslide displacement, *Eng Geol*, 186,
- 12 91-99, 10.1016/j.enggeo.2014.11.014, 2015.
- 13 Lin, P. T.: Support vector regression: Systematic design and performance analysis, Department of Electronic Engineering,
- 14 National Taiwan University, 2001.
- 15 Liu, Z., Shao, J., Xu, W., Chen, H., and Shi, C.: Comparison on landslide nonlinear displacement analysis and prediction with
- 16 computational intelligence approaches, *Landslides*, 11, 889-896, 10.1007/s10346-013-0443-z, 2014.
- 17 Lv, Y., Liu, J., Yang, T., and Zeng, D.: A novel least squares support vector machine ensemble model for NOx emission prediction
- 18 of a coal-fired boiler, *Energy*, 55, 319-329, 10.1016/j.energy.2013.02.062, 2013.
- 19 Marjanović, M., Kovačević, M., Bajat, B., and Voženilek, V.: Landslide susceptibility assessment using SVM machine learning
- 20 algorithm, *Eng Geol*, 123, 225-234, 10.1016/j.enggeo.2011.09.006, 2011.
- 21 Micheletti, N., Foresti, L., Kanevski, M., Pedrazzini, A., and Jaboyedoff, M.: Landslide susceptibility mapping using adaptive
- 22 support vector machines and feature selection, *Geophys Res Abstr*, EGU, 13, 2013.
- 23 Min, J. H., and Lee, Y.: Bankruptcy prediction using support vector machine with optimal choice of kernel function parameters,
- 24 *Expert Syst Appl*, 28, 603-614, 10.1016/j.eswa.2004.12.008, 2005.
- 25 Miyagi, T., Yamashina, S., Esaka, F., and Abe, S.: Massive landslide triggered by 2008 Iwate-Miyagi inland earthquake in the
- 26 Aratozawa Dam area, Tohoku, Japan, *Landslides*, 1, 99-108, 10.1007/s10346-010-0226-8, 2011.
- 27 Nefeslioglu, H. A., Gokceoglu, C., and Sonmez, H.: An assessment on the use of logistic regression and artificial neural networks
- 28 with different sampling strategies for the preparation of landslide susceptibility maps, *Eng Geol*, 97, 171-191,
- 29 10.1016/j.enggeo.2008.01.004, 2008.
- 30 Pourbasheer, E., Riahi, S., Ganjali, M. R., and Norouzi, P.: Application of genetic algorithm-support vector machine (GA-SVM)
- 31 for prediction of BK-channels activity, *Eur J Med Chem*, 44, 5023-5028, 10.1016/j.ejmech.2009.09.006, 2009.
- 32 Pradhan, B., Abokharima, M. H., Jebur, M. N., and Tehrany, M. S.: Land subsidence susceptibility mapping at Kinta Valley
- 33 (Malaysia) using the evidential belief function model in GIS, *Nat Hazards*, 73, 1019-1042, 10.1007/s11069-014-1128-1, 2014.
- 34 Ren, F., Wu, X., Zhang, K., and Niu, R.: Application of wavelet analysis and a particle swarm-optimized support vector machine
- 35 to predict the displacement of the Shuping landslide in the Three Gorges, China, *Environ Earth Sci*, 73, 4791-4804,
- 36 10.1007/s12665-014-3764-x, 2015.
- 37 Sassa, K., Picarelli, L., and Yin, Y. P.: Monitoring, prediction and early warning. In: Sassa K, Canuti P (eds) *Landslides-disaster*
- 38 *risk reduction*, Springer-Verlag, Berlin Heidelberg, 2009.
- 39 Shen, J., Karakus, M., and Xu, C.: Direct expressions for linearization of shear strength envelopes given by the Generalized
- 40 Hoek-Brown criterion using genetic programming, *Comput Geotech*, 44, 139-146, 10.1016/j.compgeo.2012.04.008, 2012.
- 41 Sun, Z., Choi, T., Au, K., and Yu, Y.: Sales forecasting using extreme learning machine with applications in fashion retailing,
- 42 *Decis Support Syst*, 46, 411-419, 10.1016/j.dss.2008.07.009, 2008.
- 43 Suykens, J.A.K., and Vandewalle, J.: Least Squares Support Vector Machine Classifiers, *Neural Process Lett* 9, 293-300,
- 44 10.1023/A:1018628609742, 1999.
- 45 Suykens, J.A.K., De Brabanter, J., Lukas, L., and Vandewalle, J.: Weighted least squares support vector machines: robustness and
- 46 sparse approximation, *Neurocomputing*, 48, 85-105, 10.1016/S0925-2312(01)00644-0, 2002.



- 1 Turner, D., Lucieer, A., and de Jong, S.: Time series analysis of landslide dynamics using an unmanned aerial vehicle (UAV),
- 2 Remote Sens-Basel, 7, 1736-1757, 10.3390/rs70201736, 2015.
- 3 Vandenberghe, F., and Engelbrecht, A. P.: A study of particle swarm optimization particle trajectories, Inform Sciences, 176,
- 4 937-971, 10.1016/j.ins.2005.02.003, 2006.
- 5 Vapnik, V.: The nature of statistical learning theory, Springer Verlag, New York, 1995.
- 6 Wang, J. F.: Quantitative prediction of landslide using S-curve, Chin J Geol Hazard Control, 14, 3-10, 2003(in Chinese).
- 7 Wang, Y., Yin, K. L., and An, G. F.: Grey correlation analysis of sensitive factors of landslide, Rock Soil Mech, 25, 91-93, 2004(in
- 8 Chinese).
- 9 Xu, H., and Chen, G.: An intelligent fault identification method of rolling bearings based on LSSVM optimized by improved PSO,
- 10 Mech Syst Signal Pr, 35, 167-175, 10.1016/j.ymssp.2012.09.005, 2013.
- 11 Yao, W., Zeng, Z. G., Lian, C., and Tang, H. M.: Ensembles of echo state networks for time series prediction. In: Sixth
- 12 international conference on advanced computational intelligence, Hangzhou, China, 299-304, 2013.
- 13 Yin, X., and Yu, W.: The virtual manufacturing model of the worsted yarn based on artificial neural networks and grey theory,
- 14 Appl Math Comput, 185, 322-332, 10.1016/j.amc.2006.06.117, 2007.
- 15 Zhang, H., Luo, Y.Y., Zhang, L.T., and Chen, Z.: Cultivated land change forecast based on genetic algorithm and least squares
- 16 support vector machines, Transactions of the Chinese Society of Agricultural Engineering, 25, 226-231, 2009.
- 17 Zhang, W., Niu, P., Li, G., and Li, P.: Forecasting of turbine heat rate with online least squares support vector machine based on
- 18 gravitational search algorithm, Knowl-Based Syst, 39, 34-44, 10.1016/j.knosys.2012.10.004, 2013.
- 19